Korean J. Chem. Eng., 33(2), 456-464 (2016)
DOI: 10.1007/s11814-015-0145-4

pISSN: 0256-1115
eISSN: 1975-7220

Graphene-ZnO nanocomposite for highly efficient photocatalytic degradation of methyl orange dye under solar light irradiation

Venkata Ramana Posa*, Viswadevarayalu Annavaram*, Janardhan Reddy Koduru, Varada Reddy Ammireddy***, and Adinarayana Reddy Somala*,†**

*Department of Material Science & Nanotechnology, Yogi Vemana University, Kadapa, A. P., India
**Graduate School of Environmental Studies, Kwangwoon University, Seoul 139-701, Korea
***Department of Chemistry, Sri Venkateswara University, Tirupati, A. P., India
(*Received 23 December 2014 • accepted 5 July 2015*)

Abstract−A facile synthesis of graphene oxide-zinc oxide nanocomposite (GO-ZnO) was performed by using wet chemical method of graphene oxide and zinc acetate precursors. The nanocomposite was characterized and intercalated with Raman spectroscopy, FE-SEM, TEM, SAED and EDAX. The crystalline nature was studied from P-XRD, and surface area of the sample was analyzed by BET. The chemical composition was explained in the light of XPS phenomenon. The photo electron-excitation (PL) studies were conducted for understanding the photocatalytic mechanism, and photocatalytic degradation of methyl orange was studied by using UV-VIS spectrophotometer. We investigated the photocatalytic activity involving GO-ZnO nanocomposite besides checking the re-stability of the composite. Significant high-performance photocatalytic activity of GO-ZnO nanocomposite was exhibited on methyl orange degradation under solar light.

Keywords: Nanocomposite, ZnO Cubic Voids, Photo Degradation, Methyl Orange Dye, Solar Light Irradiation

INTRODUCTION

Nanometer-sized materials have attracted growing attention for their unique physical and chemical properties [1,2]. Nanometer-sized metal oxides exhibit intrinsic surface reactivities and large surface areas; therefore, they strongly adsorb many substances including trace metals. In general, the photocatalytic activity of the catalyst is altered by the particle size, crystal structure, band gap and the hydroxyl groups. The two facts of catalyst restricted its catalytic efficiency. Charge carrier recombination occurs within a short time as nanoseconds and the band edge absorption threshold does not allow the utilization of solar light. So, it is very important to prevent the electron-hole pair form recombination for enhancing the photo catalysis efficiency [3]. Many works have been devoted to reducing the recombination of charge carriers by coupling the photocatalysts with other materials, such as noble metals [4,5], semiconductors [6] and carbon nanotubes [7].

Among various carbon nanostructures, graphene as a single-atom thick sheet arranged by sp^2-bonded carbon atoms in a hexagonal lattice shows unique properties for fundamental research [8-11]. The research in graphene-based subjects has been substantial after empirical discovery of graphene sheets in 2004 [12]. Graphene has a very large theoretical surface area (2,620 $m^2 g^{-1}$) with potential low manufacturing cost. This attribute makes it a promising material for practical applications in environmental pollutant management [13-15]. However, it is generally difficult to maintain the large surface area of graphene because of the strong van der Waals interaction between them [16]. Modified graphite oxides have been studied in the removal of metals from water [17-19] and in the removal of various gaseous air pollutants from the atmosphere [20-29]. The modification of physical properties and surface chemistry of graphite oxide enhanced its interactions with target pollutants. Recently, various metal/metal oxide-GO composites have been widely used as biosensors, capacitors and photocatalysts [30-32]. However, ZnO is considered to be a suitable alternative to TiO_2 because of its strong oxidizing power, nontoxicity, and being relatively inexpensive. Its wide band gap (3.37 eV) and higher electron mobility hamper it as a photocatalyst [33-36,37-40]. Moreover, GO/Zinc hydroxide composites [41] showed photocatalytic activity significantly enhancing the reactive adsorption of various gases on these materials [42]. In photocatalysis, ZnO can act as a photocatalyst while graphene acts as an electron-acceptor/transport material to facilitate the migration of photo generated electrons and hinders the electron-hole recombination [43,44]. As an environmental-friendly and efficient agent, ultraviolet (UV)-assisted photocatalytic reduction of GO using semiconductor oxides, typically ZnO, has been applied to synthesize graphene-based composite materials [45,46].

In this work, we have successfully fabricated GO-ZnO nanocomposites via wet chemical method and investigated their photocatalytic performances and re-stability of GO-ZnO nanocomposite material with methyl orange under solar light irradiation. The effect of different contents of GO in the GO-ZnO nanocomposites on the photocatalytic performance was also studied. The results showed enhanced photocatalytic activity of GO-ZnO nanocomposite with

†To whom correspondence should be addressed.
E-mail: anreddyphd@gmail.com

more stability.

EXPERIMENTAL SECTION

1. Preparation of Graphene Oxide

Natural graphite flakes (+100 mesh) and Methyl Orange were commercially obtained from Sigma-Aldrich. In addition, zinc acetate ($ZnC_4H_6O_4{\cdot}2H_2O$), hydrochloric acid (HCl), sulfuric acid (H_2SO_4), hydrogen peroxide (H_2O_2), potassium permanganate ($KMnO_4$), sodium hydroxide (NaOH), sodium nitrate ($NaNO_3$) were purchased from Merck and used without further purification. The ethanol used in the synthesis was supplied by China Medicine Co Ltd, and throughout the experiment double-distilled water was used.

Graphene oxide was prepared by the modified Hummers method [47]. In a typical synthesis, 10 g of graphite flakes was added to 230 mL of concentrated H_2SO_4, and these two were mixed by magnetically stirring in an ice bath. Then, 40 g of $KMnO_4$ was added slowly to the above mixture with stirring and cooling for 1.5 h. Subsequently 5 g of $NaNO_3$ was added to the above mixture, so that the temperature of the mixture was maintained below 15 °C during that time. Further oxidation was carried out by adding 30% of H_2O_2 at 98 °C in oil bath. The mixture solution was vigorously agitated for another 10 min and then centrifuged at a high speed of 14,000 rpm. The product was washed repeatedly with HCl (5%) and distilled water until the pH value of the product arrived at near 7. Then the product was dried in an air oven at 60 °C to obtain graphene oxide.

2. Synthesis of Graphene Oxide-zinc Oxide Composite

The GO-ZnO nanocomposite was synthesized by wet chemical method [48]. Graphite oxide was dispersed in ethanol (2 mg/1 mL) and sonication for 1 hour under ambient conditions. Subsequently, 0.880 g of zinc acetate ($ZnC_4H_6O_4{\cdot}2H_2O$) was dissolved into the mixture while stirring. Then, a predetermined amount of NaOH solution was added to the mixture and pH of the solution was adjusted to 10, after being stirred for 30 min. The mixture was then transferred to a 100 mL round bottom flask and heated to 140 °C under N_2 atmosphere for 24 hours. The prepared composites were then centrifuged and washed by distilled water for several times. The product was dried in a vacuum oven for 24 h at 60 °C. A simple chemical approach was employed for the GO-ZnO nanocomposite in ethanol medium, as shown in Fig. 1.

3. Characterization

The structure and morphology of the samples were characterized by X-ray diffractometer (XRD) Bruker D8 using CuKα1 (1.5406 Å) and Kα2 (1.54439 Å) radiations. Morphology of as-obtained products was studied by field emission scanning electron microscope (FESEM) imaging with energy dispersive X-ray spectroscopy (EDAX) or (EDS) using a Carl Zeiss model Ultra 55 microscope operating at 5 and 20 kV. Structure analysis was conducted by transmission

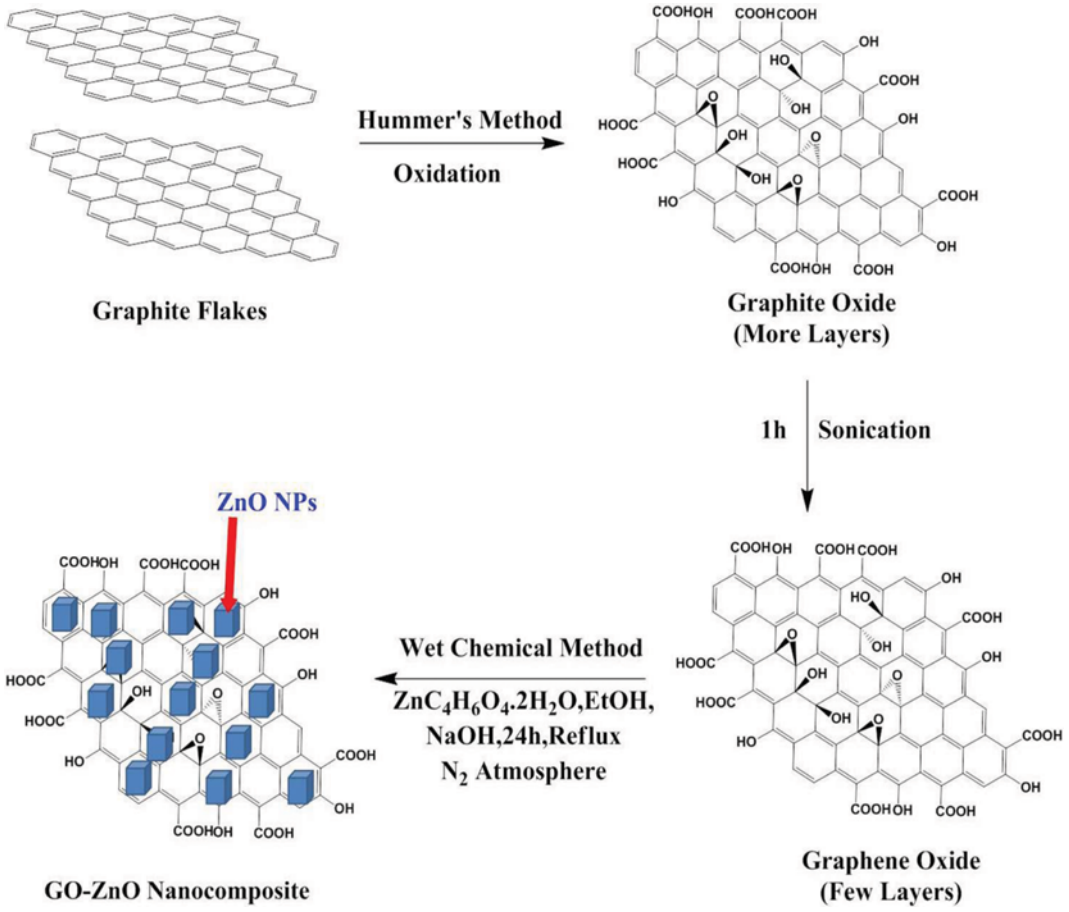

Fig. 1. The schematic representation of the chemical route of GO-ZnO nanocomposite.

electron microscope (TEM) measurements on a Tecnai G^{2}FEI F12I at 200 kV. Ultraviolet-visible absorption spectra were recorded using UV-Vis Spectroscopy Shimadzu-1800. Raman spectra were recorded using a WiTec alpha 200 SNOM system and solar light intensity was checked by TES 1332A Lux meter. Nitrogen adsorption and desorption experiments were carried out on Micromeritics ASAP 2020 analyzer. The samples were outgassed at 150 °C for 12 h in a dynamic vacuum before physisorption measurements. The specific surface area was calculated using Brunauer Emmett Teller (BET) method. X-ray photoelectron spectroscopy (XPS) measurements were conducted using an Omicron ESCA Probe spectrometer with unmonochromatized Al Kα X-rays (energy=1486.6 eV). The photoexcitation and luminescence (PL) studies were done using a JOBIN YVON Flurolog-3 spectrometer with an YSOW xenon flash lamp broad band source.

4. Photocatalytic Tests

Before being exposed to solar light for photocatalytic process, 50 mL of 5×10^{-5} M prepared MO solution was added to 50 mg of GO-ZnO photocatalyst. This mixture was then placed in ultrasonic water bath for 5 min to ensure good dispersion of catalyst, followed by being magnetically stirred for 1 h at room temperature to achieve equilibration of absorption and desorption between GO-ZnO and MO. After reaching equilibrium, 3 mL of suspension of was extracted to determine the initial concentration of MO solution, which was recorded as base concentration C_0. Afterwards, this mixed suspension was exposed to solar light whose intensity is one lakh lux, for 2 hours; 3 mL of the sample had to be taken in test tube for every 10, 20, 30, 60, 90 and 120 min. The suspension was centrifuged immediately to separate any suspended solid. The UV-visible spectra of the supernatant were recorded using a Shimadzu-1800 UV-visible spectrometer to determine the concentration of methyl orange at each time at 464 nm, which was denoted as C_t; we also studied the re-stability and made a comparison of photocatalysts.

RESULTS AND DISCUSSION

1. X-ray Diffraction Studies

The crystalline nature and orientation of graphite, commercial ZnO, and as-synthesized graphite oxide, and GO-ZnO nanocomposite was analyzed by powder X-ray diffraction (PXRD) as shown in Fig. 2. For graphite, an intense crystalline peak around 26.46° was observed, which represents the hexagonal graphite. After oxidation, the peak shifts to 9.92° and this significant change of peak location indicates the great expansion of d-spacing due to the introduction of oxygen functionalities (such as C-OH, C-O-C, C-OOH) of graphite oxide. All the samples exhibit analogous diffraction peaks in terms of ZnO framework. The dominant peaks located at ca. 31.73, 34.37, 36.21, 47.48, 56.53,62.77, 66.30, 67.86, 69.00, 72.46, and 76.86° are indexed to (100), (002), (101), (102), (110), (103), (200), (112), (201), (004), and (202) crystallographic planes of hexagonal ZnO (JCPDS File Card No. 89-1397) consistent with GO-ZnO composite. A small broader diffraction peak at 13° is observed in the GO-ZnO composite, which is similar to the diffraction patterns of GO (Fig. 2(d)) [34,35].

2. Raman Spectroscopy Measurements

Raman spectroscopy is a non-destructive and widely used technique to characterize graphitic materials, in particular, to deter-

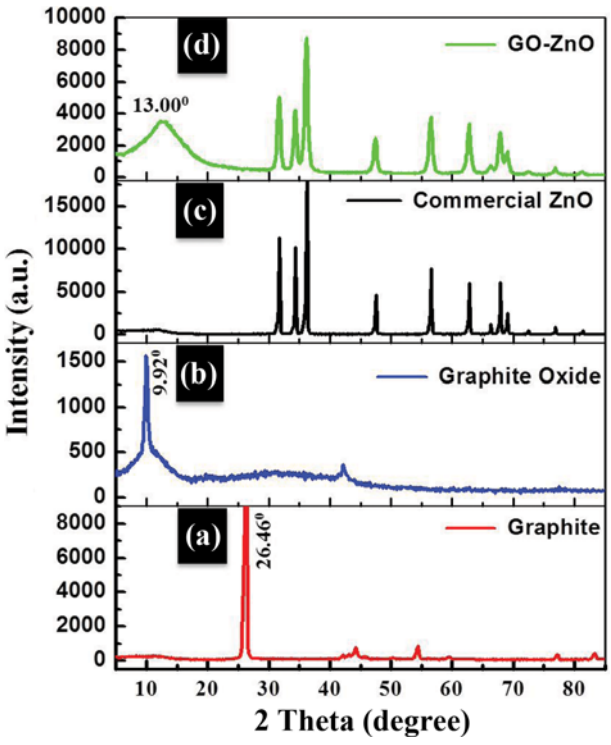

Fig. 2. PXRD patterns of (a) graphite, (b) graphite oxide, (c) commercial ZnO and (d) GO-ZnO nanocomposite.

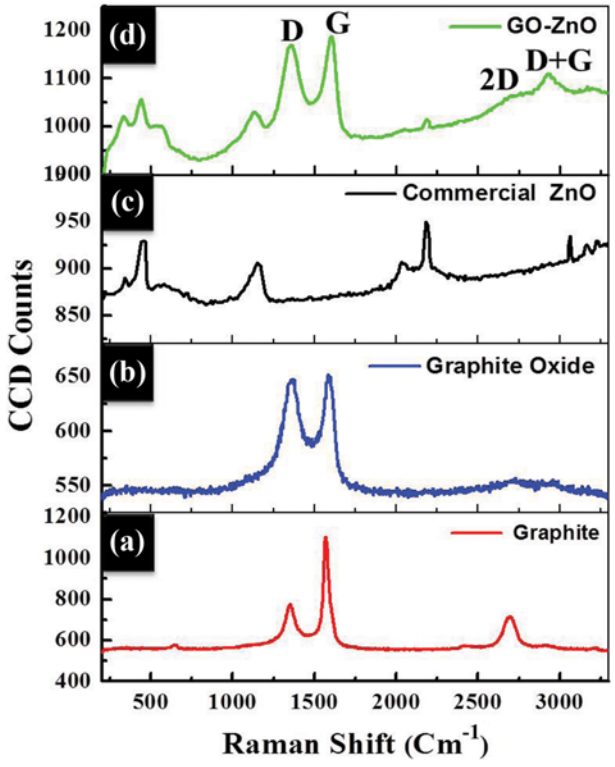

Fig. 3. Raman spectrum of (a) graphite, (b) graphite oxide, (c) commercial ZnO and (d) GO-ZnO nanocomposite.

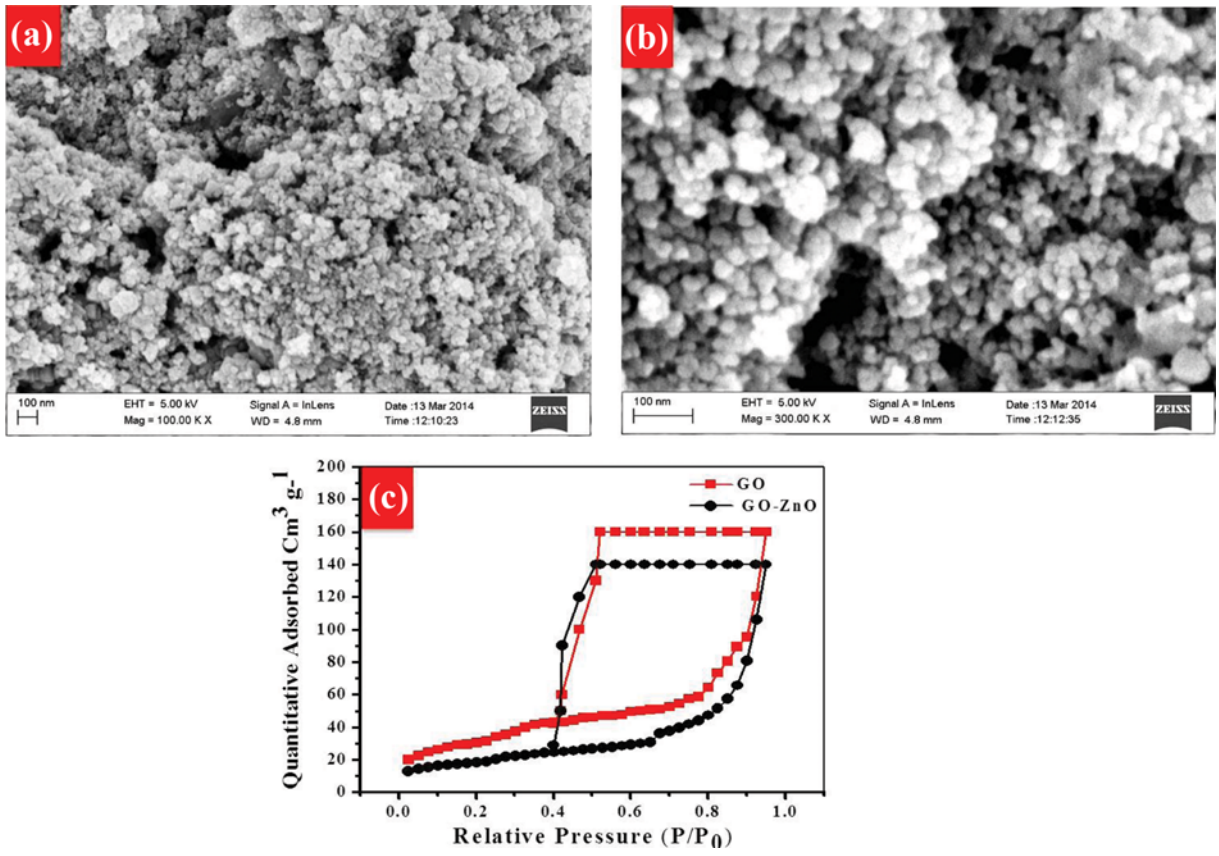

Fig. 4. FESEM images of GO-ZnO nanocomposite: (a) Low magnification and (b) high magnification and (c) N_2 adsorption-desorption isotherms of GO and GO-ZnO.

mine ordered and disordered crystal structures of graphene. Fig. 3 shows the Raman spectra of graphite, graphite oxide, commercial ZnO and GO-ZnO nanocomposite. The presence of both carbon and ZnO can be confirmed from the Raman spectra. In Fig. 3, the spectrum for ZnO displays a peak at 342 cm^{-1} which is assigned to the second-order Raman spectrum arising from zone-boundary photons of hexagonal ZnO. The intensity peak at 452 cm^{-1} corresponds to E2 (HI) mode, which is the characteristic peak of the hexagonal ZnO. The peak at 583 cm^{-1} is assigned to E1 longitudinal optical (LO) mode, attributed to oxygen deficiency defects in ZnO [49]. The peak at 1,149 cm^{-1} is due to the multiple-photon scattering processes [50]. The intensity of these peaks is reduced in composites as compared to that in ZnO due to the interaction of the ZnO and GO. From Fig. 3(a), (b) and (d), the prominent peaks of GO-ZnO at 1,361 and 1,607 cm^{-1} correspond to the well documented D band and G band, respectively. Where G band refers to the sp^2 carbon-type structure and D band refers to the presence of disorder in the graphene structure for GO and nanocomposites suggest that the structure of GO is maintained in the composites. It is reported that pristine graphite shows a sharp G band varying from 1,570 to 1,584 cm^{-1}, and a weak D band from 1,328 to 1,352 cm^{-1} [34-36,50]. The G band peak for GO is shifted towards longer wave number compared to that of pristine graphite, due to the presence of isolated double bonds in GO that resonate at frequencies higher than that of the G band of graphite [51,52]. The peak at 2,703 cm^{-1} corresponds to the overtone of the D band, and the peak at 2,923 cm^{-1} is associated with the D+G band [53]. Note that a G band up-shift from 1,584 to 1,607 cm^{-1} is observed for GO-ZnO nanocomposite with graphite oxide, which is generally viewed as evidence of chemical doping of the carbon materials [54].

3. FE-SEM Micrographs & BET Analysis

GO-ZnO was prepared by wet chemical method under nitrogen atmosphere at 140 °C for 24 h. The morphology of the synthesized GO-ZnO composite was studied by FE-SEM images (Fig. 4(a) low magnification and Fig. 4(b) high magnification). It is clearly observed that the surface of curled GO nanosheet is packed densely by ZnO nanoparticles, which displays a good combination between GO and ZnO. N_2 adsorption-desorption isotherms of GO and GO-ZnO nanocomposite is shown in Fig. 4. Specific surface areas of GO and GO-ZnO were measured by the multipoint BET method. Surface area of GO-ZnO (158.0 $m^2 g^{-1}$) was lower than that of GO (186.5 $m^2 g^{-1}$) due to the high density and low surface area of ZnO cubic voids.

4. TEM Micrographs Study

The TEM image of GO-ZnO in Fig. 5((a) and (b)) clearly indicates that the GO sheets are decorated by ZnO nanoparticles. The GO sheets act as bridges for the connection between different ZnO nanoparticles, which can significantly increase the separation of photo-generated carriers and enhance the photocatalytic performance. From Fig. 5((a) and (b)) a white particle indicates the hexagonal arrangement of graphene oxide and black particles indicate the cubic ZnO nanoparticle.

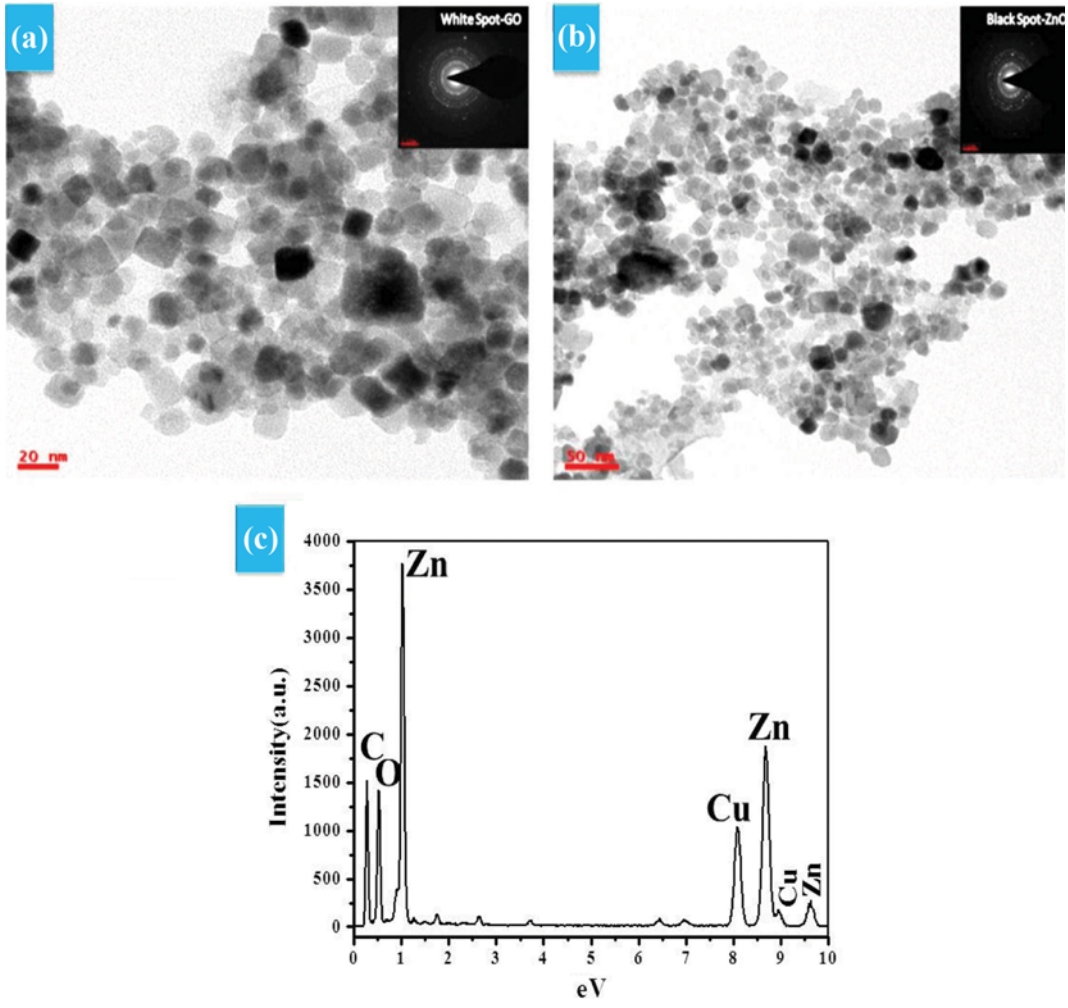

Fig. 5. TEM images (a) & (b) of GO-ZnO nanocomposite with inside SAED pattern of the GO and ZnO, (c) EDAX results of GO-ZnO nanocomposite.

Selective area electron diffraction (SAED) pattern of hybrid material shows the fusion of super lattices characteristic of the layer structure of any kind of materials. When we selectively focused the electron beam on a hybrid material, we found that apart from the super lattices we also observed cubic arrangement of ZnO (inside Fig. 5(b)) and hexagonal arrangement of GO (inside Fig. 5(a)). Fig. 5(c) shows the energy dispersive absorption x-ray spectrum (EDAX) results of the GO-ZnO nanocomposite. Zn, O, C and Cu elements are observed. The Cu element is observed because the EDAX test was performed using HRTEM with a Cu mesh substrate.

5. HR-TEM Micrographs Measurements

An HR-TEM image of the GO-ZnO nanocomposite shows springs/curled in 5 nm range, which is usually observed only in the case of material that is crystalline. From the P-XRD it is observed the crystalline nature of the GO-ZnO nanocomposite as well as graphene oxide was confirmed by HRTEM. When focused on GO and ZnO individually, HRTEM results observed the springs on the both layers as in hexagonal arrangement (GO) and cubic form which are shown in Fig. 6.

6. XPS Analysis

X-ray photoelectron spectroscopy (XPS) analysis was used to explore the chemical states of elements in the GO-ZnO nanocomposites. The obtained data were calibrated by using the adventitious carbon at a binding energy of 284.6 eV. The analysis spectrum Fig. 6(a) indicates that the sample is composed of Zn, O and C, and no peaks of other elements were observed. The two peaks detected at the energy positions of 1,010-1,050 eV correspond to the Zn 2p3/2 and Zn 2p1/2 orbitals. The high-resolution scan of Zn 2p, shown in Fig. 7(b), identifies the exact peak location of Zn 2p3/2 at 1,022.7 eV and of Zn 2p1/2 at 1,045.7 eV. In Fig. 7(c), the O 1s profile is asymmetric and can be fitted to two symmetrical peaks at 530.9 and 532.3 eV, respectively, indicating two different types of oxygen species in the sample. The two peaks are associated with the lattice oxygen of ZnO and chemisorbed oxygen caused by the surface hydroxyl. The deconvoluted C 1s XPS spectrum Fig. 7(d) shows three peaks at 285.0, 286.2 and 289.1 eV. The binding energy at 285.0 eV is assigned to the C-C bond (sp^2) of grapheme oxide. The peak at 286.2 eV is ascribed to the C-O bond, while the peak at 289.1 eV is assigned to the C=C bond [55].

7. Photoluminescence (PL) Spectral Studies

Photoluminescence spectra of GO-ZnO and ZnO are shown in Fig. 7 A. The emission intensity considerably decreases with the

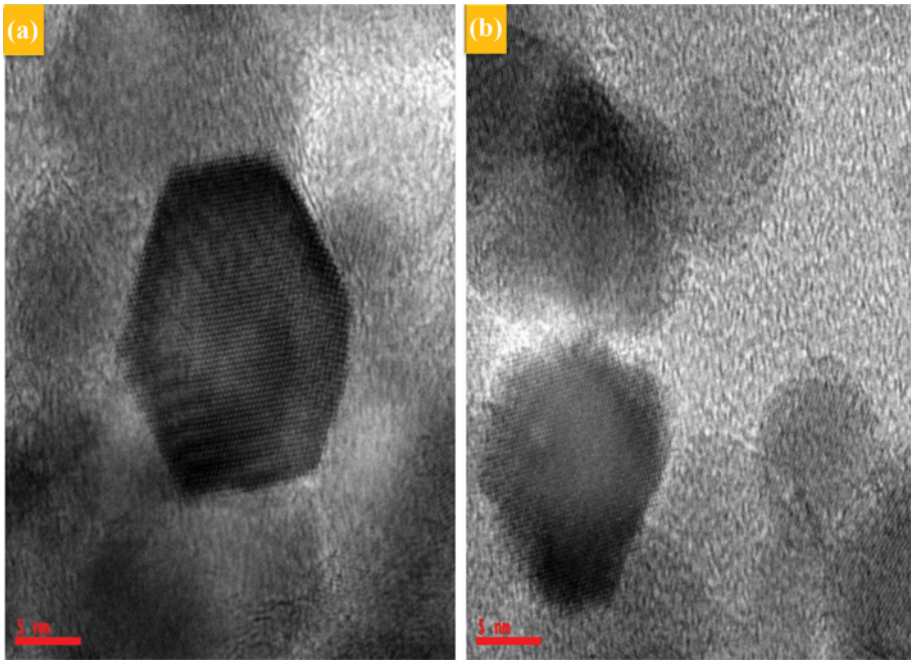

Fig. 6. HRTEM images of (a) GO and (b) ZnO.

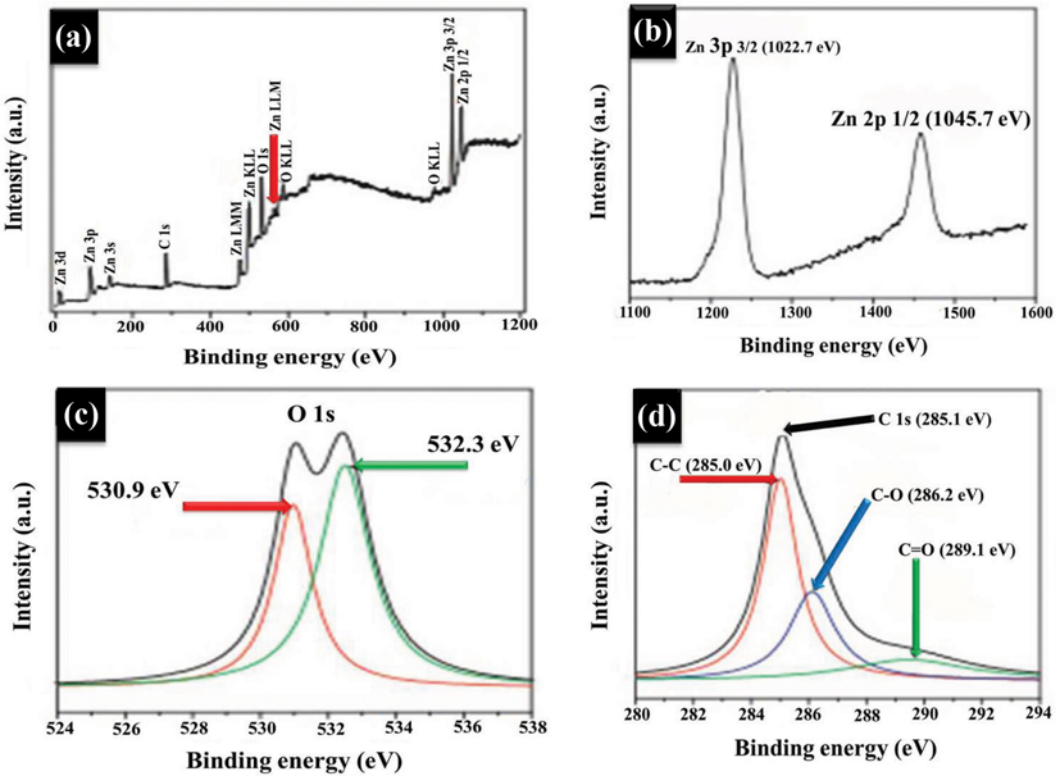

Fig. 7. (a) XPS analysis spectra, (b) high resolution spectra of Zn 2p region, (c) O 1s region and (d) C 1s region for GO-ZnO nanocomposite.

GO-ZnO, implying that the recombination of photogenerated carriers was effectively inhibited. The PL intensity of ZnO is the highest, indicating the high probability of recombination of electrons and holes. ZnO is a good electron donor, and graphene materials are comparatively good electron acceptors; the synergistic effect between these two components would excellently reduce recombination and lead to an increased charge carrier separation.

8. Photocatalytic Degradation of Methyl Orange Dye

It is well known that the photo-catalytic degradation of the organic pollutants follows the pseudo-first-order kinetic [56], which exhib-

its a linear relationship between $\ln(C_0/C_t)$ and the reaction time. The kinetics equation of the first-order reaction can be described as **ln C_0/Ct=Kt**, where, C_0 is the initial concentration of MO, t the reaction time and C_t the concentration of MO at reaction time of t. So based on the first-order equation, the activities of the photocatalysts are determined by measuring the absorbency of the MO in solution at a certain time intervals. The hybrid material of GO-ZnO has good surface area and shows the absorption various organic reactive intermediates which are pollutant to the atmosphere. It can also absorb the other organic species. To demonstrate the photocatalytic effect of GO-ZnO nanocomposite toward a more stable organic dye, the photodegradation of MO in water under the sun-

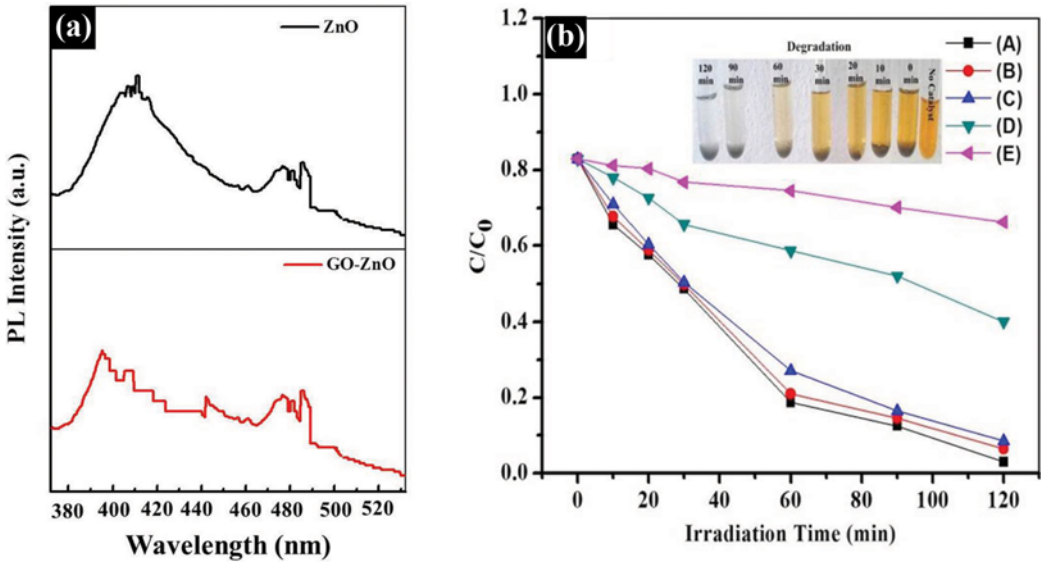

Fig. 8. (a) PL spectra of ZnO and GO-ZnO with excitation wavelength of 325 nm (b) three cycles (a), (b), (c) of photocatalytic degradation of MO with GO-ZnO nanocomposite as catalyst and comparison of (d) ZnO and (e) GO.

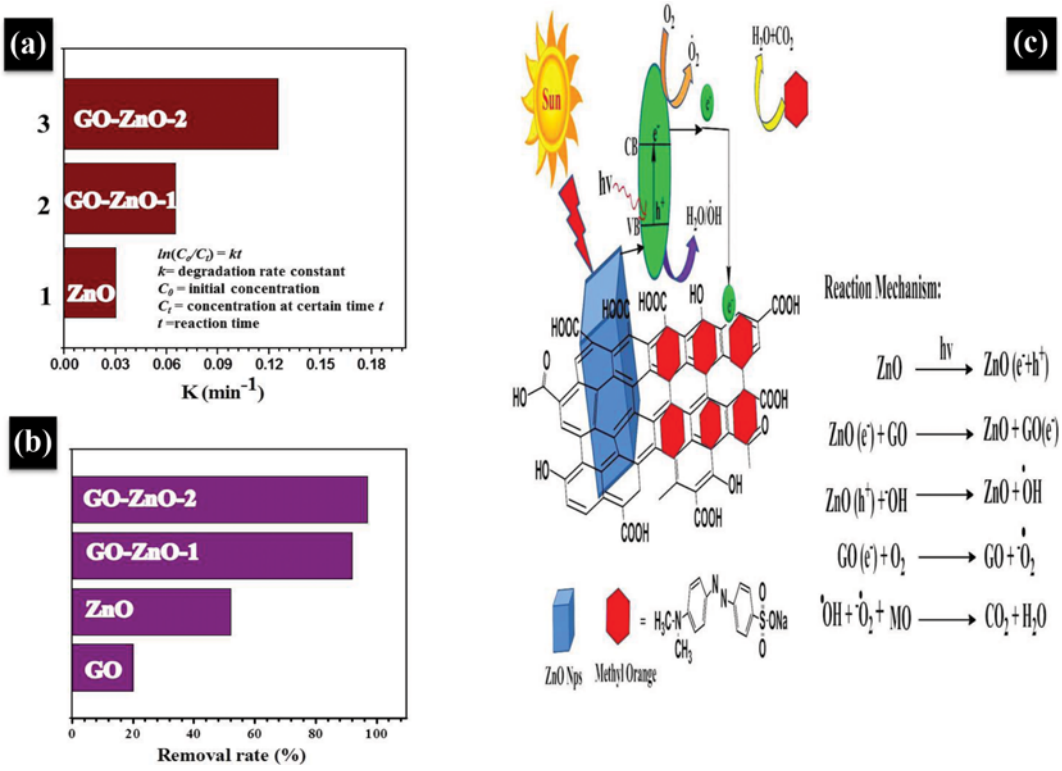

Fig. 9. The reaction rate constant of MO photodegradation in the presence of different concentration catalysts, (b) the removal rate of MO for solar light irradiation at 120 min with GO, commerial ZnO and GO-ZnO-1 and GO-ZnO-2 (c) possible mechanism of photosensitized degradation of MO over GO-ZnO nanocomposite under solar light.

light irradiation was carried out at regular time intervals. The absorption of these solutions decreased gradually with irradiation time (i.e., the characteristic absorption of MO almost disappeared after about 120 min, and the color of MO solution changed gradually from light orange to colorless after irradiation for 120 min); photodegradation of MO solution with GO-ZnO nanocomposite, ZnO and GO is shown in the Fig. 8(b). The first run of GO-ZnO calculates the MO degradation is 97% and likewise calculates the MO degradation of ZnO and GO is 52% and 21%, respectively, suggesting that GO-ZnO is a high-quality catalyst. The stability of photocatalyst during photocatalytic reaction is a crucial factor for practical applications. To test the reusability of GO-ZnO nanocomposite in MO photodegradation, three cycles of the photocatalytic experiment for GO-ZnO nanocomposite were carried out. As shown in Fig. 8(b), MO could be totally decomposed in each cycle and the GO-ZnO photocatalyst exhibited almost no change in its photocatalytic activity during the repeated photocatalytic experiments. Thus, the higher photocatalytic activity and restability/reusability of GO-ZnO nanocomposite were beneficial for its application as a photocatalyst.

Fig. 9(a) shows the reaction rate constant (k (MO)) for different catalysts. The results show that the rate constant for GO-ZnO-2 composite (k (MO)=0.024/min) was much higher than that of commercial ZnO (k (MO)=0.008/min). The significantly enhanced photocatalytic performance of GO-ZnO composites under sunlight is attributed to the band gap narrowing of the composite material, which can allow more absorption of solar light as well as more efficient transfer of photogenerated electrons from excited MO to ZnO nanoparticles through graphene nanosheets. Fig. 9(b) shows the removal rate of MO in 120 min for commercial ZnO and GO-ZnO nanocomposites. Exclusively, when the amount of GO is 10 wt%, the resultant GO-ZnO nanocomposite shows the highest photocatalytic performance. However, with further increase of the GO content above 10 wt%, the photocatalytic activity decreases slightly. These findings indicate that the introduction of GO into ZnO plays an important role in the absorption capacity and photocatalytic performance of the GO-ZnO nanocomposites. The graphene amount is further increased above its optimum value, and the photocatalytic performance deteriorates. Photocatalytic performance reduces because graphene can absorb light, and the excessive graphene can act as a kind of recombination center instead of providing an electron pathway.

The photocatalytic degradation of organic dyes by semiconductor under sunlight irradiation generally involves two mechanisms. The first is based on the excitation of the semiconductor, which involves excitation of the semiconductor by light irradiation to form photogenerated electrons in the conduction band and holes in the valence band, and the subsequent chemical reactions with the surrounding media after the photo generated charges move to the particle surface. The other mechanism is based on the excitation of dye, in which the dye acts as a sensitizer of visible light as well as injects excited electrons to an electron acceptor to become a cationic dye radical (dye^{*+}), followed by self-degradation or degradation by the reactive oxidation species [57]. When GO-ZnO nanocomposites are irradiated by sunlight, electrons (e^-) will transfer from valence band (VB) to the conduction band (CB) and leave positive holes (h^+) in VB in ZnO. Due to the lower Fermi level, delocalized conjugated structure and superior electrical conductivity of GO, the sunlight generated electrons in ZnO are preferentially transferred to GO, leaving the reactive holes behind in the ZnO. The GO in GO-ZnO nanocomposite system preferentially accepts the photogenerated electrons as an electron reservoir. The high charge separation efficiency of e^-/h^+ pairs significantly decreases the chances of recombination rate of ZnO, effectively prolongs the lifetime of holes in ZnO and makes it easier for photogenerated electron and holes to participate radical reactions, thus increasing the photocatalytic efficiency dramatically. Dissolved oxygen (O_2) adsorbed on the surface of GO-ZnO nanocomposites can react with e^- to form superoxide radical ($\cdot O_2^-$), and hydroxyl ions (OH^-) will be oxidized into hydroxyl radicals (^-OH) by h^+. MO can be degraded into simple organics and further into CO_2 and H_2O by those $\cdot O_2^-$ and ^-OH radicals. The typical reaction steps in the photocatalytic degradation under sun light irradiation are shown in Fig. 9(c).

CONCLUSION

GO-ZnO nanocomposite was successfully synthesized via chemical route method. The experimental results indicate that (i) GO-ZnO nanocomposite exhibits high-quality photocatalytic performance; (ii) GO-ZnO has good re-stability/re-usability photocatalyst; and (iii) the high photocatalytic performance is ascribed to the increased light absorption intensity and range as well as the reduction of photoelectron-hole pair recombination in ZnO with the introduction of GO-ZnO nanocomposite achieves a highest methyl orange removal rate of 97%. Our findings provide necessary information to understand the mechanism in enhanced photocatalytic property in GO-ZnO system and to guide further research for effective and efficient photocatalysts.

ACKNOWLEDGEMENT

This work was financially supported by University Grant Commission, New Delhi [Grant no.2-362/2013 (SR)] and instrumental analysis supported by University of Hyderabad, S.V. University and IIT Madras is gratefully acknowledged. We are also thankful to Dr. R. V. Jayanth Kasyap, Asst. Professor in English, Yogi Vemana University, Kadapa, India for verifying the linguistic correctness.

REFERENCES

1. M. Soylak and N. D. Erdogan, *J. Harzard. Mater.*, **137**, 1035 (2006).
2. O. D. Uluozlu, M. Tuzen, D. Mendil and M. Soylak, *J. Harzard. Mater.*, **176**, 1032 (2010).
3. J. Qin, X. Zhang, Y. Xue, N. Kittiwattanothai, P. Kongsittikul, N. Rodthongkum, S. Limpanart, M. Ma and R. Liu, *Appl. Surf. Sci.*, **321**, 226 (2014).
4. M. Seredych, O. Mabayoje and T. J. Bandosz, *J. Phys. Chem. C*, **116**, 2527 (2012).
5. M. Seredych, O. Mabayoje, M. M. Kolesnnik, V. Krstic and T. J. Bandosz, *J. Mater. Chem.*, **22**, 7970 (2012).
6. T. Tatsuma, S. Saitoh, P. Ngaotrakanwiwat, Y. Ohko and A. Fujishima, *Langmuir*, **18**, 7777 (2002).

7. K. Woan, G. Pyrgiotakis and W. Sigmund, *Adv. Mater.*, **21**, 2233 (2009).
8. K. S. Novoselov, A. K. Geim, S. V. Morozov, D. Jiang, M. I. Katsnelson, I. V. Grigorieva, S. V. Dubonos and A. A. Firsov, *Nature*, **438**, 197 (2005).
9. J. C. Meyer, A. K. Geim, M. I. Katsnelson, K. S. Novoselov, T. J. Booth and S. Roth, *Nature*, **446**, 60 (2007).
10. M. I. Katsnelson and K. S. Novoselov, *Solid State Commun.*, **143**, 3 (2007).
11. F. Schedin, A. K. Geim, S. V. Morozov, E. W. Hill, P. Blake, M. I. Katsnelson and K. S. Novoselov, *Nat. Mater.*, **6**, 652 (2007).
12. K. S. Novoselov, A. K. Geim, S. V. Morozov, D. Jiang, Y. Zhang, S. V. Dubonos, I. V. Grigorieva and A. A. Firsov, *Science*, **306**, 666 (2004).
13. G. Srinivas, J. W. Burress, J. Ford and T. Yildirim, *J. Mater. Chem.*, **21**, 1323 (2011).
14. M. Seredych, O. Mabayoje and T. J. Bandosz, *Langmuir*, **28**, 1337 (2012).
15. M. Seredych, O. Mabayoje and T. J. Bandosz, *J. Phys. Chem. C.*, **116**, 2527 (2012).
16. M. J. Allen, V. C. Tung and R. B. Kaner, *Chem. Rev.*, **110**, 132 (2010).
17. S. T. Yang, Y. Chang, H. Wang, G. Liu, S. Chen, Y. Wang, Y. Liu and A. Cao, *J. Colloid Interface Sci.*, **357**, 122 (2010).
18. V. Chandra, J. Park, Y. Chun, J. W. Lee, I. C. Hwang and K. S. Kim, *ACS Nano*, **4**, 3979 (2010).
19. V. Chandra and K. S. Kim, *Chem. Commun.*, **47**, 3942 (2011).
20. C. Petit, M. Seredych and T. J. Bandosz, *J. Mater. Chem.*, **19**, 9176 (2009).
21. M. Seredych and T. J. Bandosz, *Chem. Eng. J.*, **166**, 1032 (2011).
22. M. Seredych and T. J. Bandosz, *J. Phys. Chem. C*, **114**, 14552 (2010).
23. S. Bashkova and T. J. Bandosz, *J. Ind. Eng. Chem. Res.*, **48**, 10884 (2009).
24. M. Seredych, O. Mabayoje and T. J. Bandosz, *Langmuir*, **28**, 1337 (2012).
25. Y. Matsuo, Y. Nishino, T. Fukutsuka and Y. Sugie, *Carbon*, **46**, 1162 (2008).
26. K. Morishige and T. Hamada, *Langmuir*, **21**, 6277 (2005).
27. Y. Zhao, H. Ding and Q. Zhong, *Appl. Surf. Sci.*, **258**, 4301 (2012).
28. B. Levasseur, C. Petit and T. J. Bandosz, *ACS Appl. Mater. Interfaces*, **2**, 3606 (2010).
29. C. Petit and T. J. Bandosz, *Adv. Funct. Mater.*, **20**, 111 (2010).
30. X. Zan, Z. Fang, J. Wu, F. Xiao, F. Huo and H. Duan, *Biosens. Bioelectron.*, **49**, 71 (2013).
31. L. L. Zhang, X. Zhao, M. D. Stoller, Y. Zhu, H. Ji, S. Murali, Y. Wu, S. Perales, B. Clevenger and R. S. Ruoff, *Nano Lett.*, **12**, 1806 (2012).
32. M. Zhu, P. Chen and M. Liu, *ACS Nano*, **5**, 4529 (2011).
33. Y. Bu, Z. Chen, W. Li and B. Hou, *ACS Appl. Mater. Interfaces*, **5**, 12361 (2013).
34. Y. W. Wang, A. Cao, Y. Jiang, X. Zhang, J. H. Liu, Y. Liu and H. Wang, *ACS Appl. Mater. Interfaces*, **6**, 2791 (2014).
35. S. Ameen, M. Akhtar, M. Song and H. S. Shin, *ACS Appl. Mater. Interfaces*, **4**, 4405 (2012).
36. J. Y. Li and H. Li, *Nanoscale Research Lett.*, **4**, 165 (2009).
37. J. Lee, S. C. Nam and Y. Tak, *Korean J. Chem. Eng.*, **22**, 161 (2005).
38. F. Peng, H. Zhu, H. Wang and H. Yu, *Korean J. Chem. Eng.*, **24**(6), 1022 (2007).
39. E. Hong, T. Choi and J. H. Kim, *Korean J. Chem. Eng.*, **32**(3), 424 (2015).
40. S. P. Chaudhari, A. B. Bodade and G. Niranjanrao Chaudhari, *Korean J. Chem. Eng.*, **30**(11), 2001 (2013).
41. T. Hirakawa and P. V. Kamat, *J. Am. Chem. Soc.*, **127**, 3928 (2005).
42. V. Subramanian, E. E. Wolf and P. V. Kamat, *J. Am. Chem. Soc.*, **126**, 4943 (2004).
43. C. Zhang, J. Zhang, Y. Su, M. Xu, Z. Yang and Y. Zhang, *Physica E*, **56**, 251 (2014).
44. B. Li, T. Liu, Y. Wang and Z. Wang, *J. Colloid Interface Science*, **377**, 114 (2012).
45. S. R. Kim, M. K. Parvez and M. Chowalla, *Chem. Phys. Lett.*, **483**, 124 (2009).
46. X. Zhou, T. Shi and H. Zhou, *Appl. Surf. Sci.*, **258**, 6204 (2012).
47. W. S. Hummers and R. E. Offeman, *J. Am. Chem. Soc.*, **80**, 1339 (1958).
48. Y. Bu, Z. Chen, W. Li and B. Hou, *ACS Appl. Mater. Interfaces*, **5**, 12361 (2013).
49. X. Y. Ye, Y. M. Zhou, Y. Q. Sun, J. Chen and Z. Q. Wang, *J. Nanopart. Res.*, **11**, 1159 (2009).
50. J. Guo, L. L. Ren, R. Y. Wang, C. Zhang, Y. Yang and T. X. Liu, *Composites. Part B*, **42**, 2130 (2011).
51. K. N. Kudin, B. Ozbas, H. C. Schniepp, R. K. Prudhomme, I. A. Aksay and R. Car, *Nano Lett.*, **8**, 36 (2008).
52. B. Adhikari, A. Biswas and A. Banerjee, *Langmuir*, **28**, 1460 (2012).
53. F. Wang and K. Zhang, *J. Mol. Catal. A. Chem.*, **345**, 101 (2011).
54. E. P. Gao, W. Z. Wang, M. Shang and J. H. Xu, *Phys. Chem.*, **13**, 2887 (2011).
55. M. Ahmad, E. Ahmed, Z. L. Hong, J. F. Xu, N. R. Khalid, A. Elhissi and W. Ahmed, *Appl. Surf. Sci.*, **274**, 273 (2013).
56. V. H. Luan, H. N. Tien and S. H. Hur, *J. Colloid Interface Sci.*, **437**, 181 (2015).
57. M. Ahmad, E. Ahmed, Z. L. Hong, N. R. Khalid, W. Ahmed and A. Elhissi, *J. Alloys Compd.*, **577**, 717 (2013).